

INTERACTIONS BETWEEN TIDAL TURBINE WAKES: NUMERICAL STUDY FOR SHALLOW WATER APPLICATION

Gisrina Elin Suhri^a, Anas Abdul Rahman^{a*}, Lakshuman Dass^a, Kumaran Rajendran^a, Ayu Abdul Rahman^b

^aMechanical Engineering Program, Faculty of Mechanical Engineering Technology, Universiti Malaysia Perlis, Pauh Putra Main Campus, 02600 Perlis, Malaysia

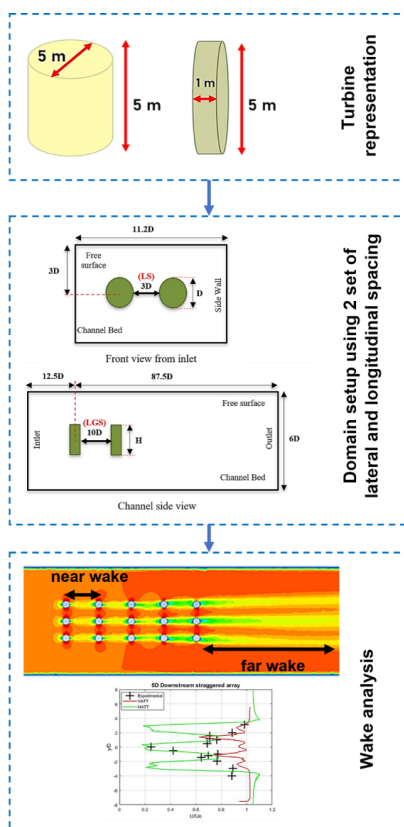
^bDepartment of Mathematics and Statistics, School of Quantitative Sciences, Universiti Utara Malaysia, 06010 UUM, Sintok, Kedah, Malaysia

Article history

Received
28 September 2021
Received in revised form
24 March 2022
Accepted
31 March 2022
Published Online
20 June 2022

*Corresponding author
anasrahman@unimap.edu.my

Graphical abstract



Abstract

The placement of tidal turbines in a tidal farm is challenging owing to the flow resistance caused by individual devices. To successfully deploy tidal turbines, the wake interaction between devices, often determined by the array's layout and spacing, must be understood. In this study, the impact of array configuration for shallow water application is examined numerically using computational fluid dynamics (CFD). This is to propose a suitable array structure for possible implementation in Malaysia. This numerical study uses 15 turbines in a staggered and squared array with two sets of lateral and longitudinal spacing combinations. The horizontal axis tidal turbine (HATT) and vertical axis tidal turbine (VATT) are represented using disc and cylindrical models, respectively. The VATT with staggered setup and greater spacing model demonstrates faster wake recovery (between 10% to 21%), compared to the squared arrangement. This meets the far wake criteria and reduces the chance of wake mixing. It is also suitable for shallow depth implementation.

Keywords: Tidal array, Staggered array, Marine energy, Turbulent mixing, Wake recovery

Abstrak

Penempatan turbin pasang surut di ladang pasang surut diketahui mencabar kerana rintangan aliran yang disebabkan oleh peranti individu. Untuk menggunakan turbin pasang surut dengan jayanya, interaksi keracak antara peranti, selalunya ditentukan oleh aturan dan jarak tatasusunan, mestilah difahami. Dalam kajian ini, impak konfigurasi tatasusunan untuk aplikasi di air cetek dikaji secara berangka menggunakan perkomputeran dinamik bendalir (CFD) bagi mencadangkan struktur tatasusunan yang bersesuaian untuk kegunaan di Malaysia. Kajian berangka ini menggunakan 15 turbin dalam tatasusunan tidak serentak dan berpetak dengan dua set gabungan jarak sisi dan membujur. Turbin pasang surut paksi mendatar (HATT) dan turbin pasang surut paksi menegak (VATT) masing-masing diwakili dengan menggunakan hipotesis model cakera 'penggerak' dan silinder. VATT dengan susunan tidak serentak dan model dengan jarak yang lebih besar menunjukkan pemulihan keracak yang lebih pantas (antara 10% hingga 21%) berbanding susunan berpetak dan memenuhi kriteria keracak jauh yang mengurangkan peluang pencampuran keracak dan sesuai untuk pelaksanaan di kedalaman cetek.

Kata kunci: Tatasusunan pasang surut, Susunan tidak serentak, Tenaga marin, Pencampuran pergolakan, Pemulihan keracak

© 2022 Penerbit UTM Press. All rights reserved

1.0 INTRODUCTION

Fossil fuels are the primary sources of energy in Malaysia. Population growth, industrial development, and technical advances have enhanced society's living standards. However, these societal advances have also increased energy usage in the country [1]. Consequently, the oil and gas industry is facing a significant dilemma. This is because oil production has reached its peak and is expected to drop significantly in the future [2]. Owing to the limited supply and production of fossil fuels, Malaysia is expected to struggle in maintaining its primary source of income and energy supply [3]. Therefore, the government has begun to explore, promote, and utilise renewable energy [4] as a conventional source of energy to decrease reliance on petroleum. These methods provide cost-effective sustainable energy with minimal environmental impacts [5].

Renewable energy can be harvested from various natural resources (such as solid waste, biomass, solar, biogas, and mini-hydro) to generate electricity [6]. Malaysia has the potential to harvest energy via hydropower resources. This is because its practical geographical location is surrounded by oceans. Moreover, it has a tropical climate and receives abundant rainfall over the year [7]. Considering the various hydropower resources in Malaysia, tidal energy technologies, particularly tidal turbines, have attracted most attention because of their simplicity and cost efficiency [4]. Compared to other hydroelectric energy sources, tidal streams have a greater energy density, are nearly invisible, and are the most constant and continuously predictable renewable energy sources available.

A tidal turbine is an underwater device which harvests energy from a flowing fluid and is often compared to wind turbine systems [8]. Both technologies operate on the same concept and have approximately identical system structures. The main difference between these two systems is the working fluid. Although it is comparable to wind energy harvesting, extracting energy from tides is more challenging to commercialise. This is because it operates under conditions of unsteady flows and complex bathymetry. It also has to cope with the effects of waves and sediment movement. Therefore, only a portion of the existing knowledge and methods from the wind energy industry can be used for tidal turbine energy systems [9].

Similar to wind turbines, tidal turbine array designs can significantly influence performance. Wake shadowing and merging across rows in an array may produce poor feedback on the farm efficiency [5]. This is caused by momentum recovery after the first row of turbines, which reduces downstream device power production and damages the entire farm [6]. A tidal turbine array must be developed, considering the spacing, layout, and quantity of devices.



Figure 1 Rev. Horns wind farm with the presence of wake shadowing [10]

Figure 1 depicts the Rev. Horns Wind Farm as an example of wake shadowing. This has caused a significant damage to the overall farm production owing to a reduced recovery of momentum after the first row of turbines [10]. The downstream devices' power generation capacity was decreased by approximately 40% compared to the front row devices at the Rev. Horns wind farm. These wind energy experiences must now be adapted into the tidal turbine array design [11]. This demonstrates the challenges in developing tidal arrays. Several parameters may influence the interaction between turbines and their wakes. These include device spacing, channel dimension, number of devices, and device arrangement [12].

Furthermore, because Malaysian open water characteristics are rather shallow (i.e., approximately 60 m in depth), the turbine cannot be placed on the seabed because the depth of the water column is too shallow for the device to function properly [13]. Because the implementation of tidal energy in Malaysia is currently minimal, important parameters (such as array size, device positioning, device spacing, and array layout), which influence tidal turbine performance, are not very well understood. Hence, this study aims to explore potential tidal turbine array layouts and setups that can match Malaysia's ocean conditions.

2.0 METHODOLOGY

To explore the fluid flow behaviour, particularly turbulent flows, a numerical model using the Reynolds-averaged-Navier-Stokes (RANS) equations is used in the ANSYS Fluent CFD package. Compared to other approaches such as large eddy simulation (LES) and direct numerical simulations (DNS), the RANS approach offers lower computing costs and a shorter processing time [14]. In addition, owing to the limited data and the high cost of the experimental study, this approach is a viable way to obtain more comprehensive information on wake behaviour. The numerical simulation consists of three main steps: pre-processing (geometry, generation of grid, and numerical setting), processing (solver), and post-processing (result). The RANS approach is expressed as shown in Eq. (1):

$$\rho \frac{\partial u}{\partial t} + \rho u \cdot \nabla u = -\nabla p + \mu \nabla^2 u - \nabla \cdot (\rho u' u') + Su, \tag{1}$$

where the mean velocity is denoted by u , u' represents the fluctuating velocity, p is the pressure, μ represents the dynamic viscosity, and Su indicates the momentum term. Reynolds stress tensor $\rho u' u'$ will appear on the right side of the final equation [15]. It describes the turbulent fluctuations in the flow. It is defined for incompressible flows as:

$$\rho u' u' = T_R = -\frac{2}{3} k \rho I + \mu_T (\nabla u + (\nabla u)^T), \tag{2}$$

where $k = (u' u')/2$ represents the turbulent kinetic energy, and μ_T represents the dynamic eddy viscosity. Turbulence simulation using CFD is normally performed using the $k-\epsilon$ (k-epsilon) model [16]. This is a two-equation model that provides two additional transport equations to represent the turbulent flow. Convection and turbulent energy diffusion may be accounted for in a two-equation model [17]. Both turbulent kinetic energy (k) and dissipation (ϵ) are important factors in turbulence [17]. The actuator disc method depicts the turbine as a simpler disc with the same rotor parameters. Thereafter, it is utilised to calculate the flow force. Forces are applied to the disc by the flow in the form of body loads or negative momentum source terms [18]. The actuator cylinder technique is similar to the actuator disc technique; however, the heights and axes are different. It presumes a uniform flow and ignores the influence of individual blades and swirls [19].

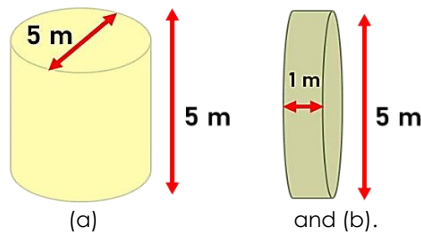


Figure 2 Dimensions of tidal devices used in this study: (a) Cylindrical shape to represent VATT (b) Circular/disc shape to represent HATT

However, this study employs a hypothetical “actuator” cylinder and disc, where instead of calculating the negative momentum source term, physical objects in the form of cylinders and discs are used to represent the turbines. Figure 2 shows a schematic of the dimensions of the turbine model used in this study.

To set up the array, two sets of different separation distances were used to organise 15 turbines in a staggered and squared manner. The turbines in the staggered array are placed in rows of three, with two turbines alternating between them. Each row of the three turbines is arranged in alignment with each other in a squared array as depicted in Figure 3. In

addition, the two separation sets cover two types of spacing: one set of short-distance spacing and the other set of longer-distance setups. These separation distances were chosen based on previous studies by Hoe [19], Harrison *et al.* [20], and Bakri [21]. The wake interaction generated by the turbine separation was evaluated using these two predetermined sets. Table 1 lists the dimension parameters used for the separation.

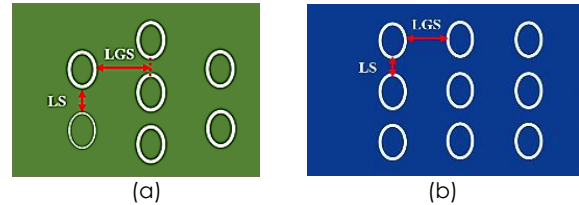


Figure 3 Turbine arrangements in the domain: (a) Staggered array (b) Squared array

Table 1 Separation distance between each turbine in the array for the two pre-determined sets

Parameters	Longitudinal Spacing, LGS (m)	Lateral Spacing, LS (m)
Set 1	3.5D	1.5D
Set 2	7.0D	3.0D

The initial stage in the simulation study was to create a graphical geometry and grid meshing process. The geometry, referred to as the simulation domain, should match the real physical or experimental conditions. This study refers to the study conducted by Harrison *et al.* [20] and Hoe [19] to establish the parameters for setting up a numerical model. Considering Figure 4, a stationary domain size of 800 m x 30 m x 80 m (L x H x W) is employed. The first row of the turbine is located 12.5 D from the inlet, where D is the diameter of the turbine.

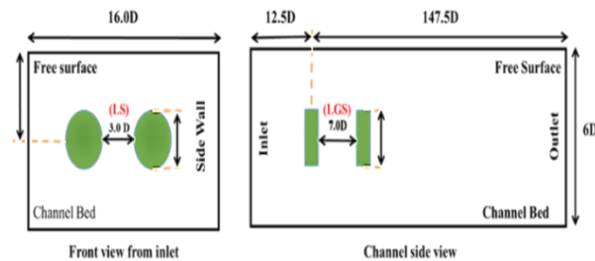
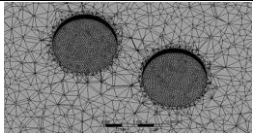
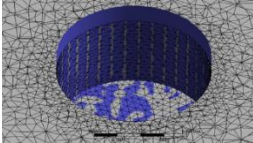
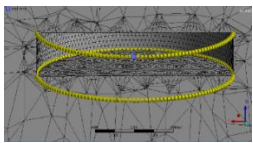


Figure 4 Simulation domain and boundary condition.

The subsequent step is the grid generation, which is often known as meshing. In general, the meshing procedure has a large impact on the computing outcomes and computational time. The mesh was created in the ANSYS Fluent CFD package with an element size of 2.0 m and a total element count of 143712 on the generated domain. Additionally, mesh refinement was applied at the faces and edges of the object (i.e., the turbine). The element size is set to be approximately 0.25 m as summarised in Table 2. Other

meshing details for both the domain and turbine models have been simplified and are presented in Table 2.

Table 2 Global and localised meshing setting applied at the overall domain and area of interest

Application	Element Size (m)	Graphical Detail
Domain's body	2.0	
Model's faces	0.25	
Model's edges	0.2	

Thereafter, the procedure was performed by setting up the following parameters. Seawater was specified as a medium with a density and dynamic viscosity of 1023 kg/m³ and 0.00093 N.s/m², respectively. The inlet, outlet, and top wall planes are defined as the boundary conditions with the specifications listed in Table 3 and are subjected to non-slip conditions. The values for all the parameters used in Table 3 are established based on previous studies for validation.

Table 3 Parameter specification for boundary condition setup

Parameters	Specification
Inflow velocity	1 m/s
Intensity of turbulent	5%
Hydraulic diameter value	0.1 m

Considering ANSYS, the three-dimensional numerical computation was performed utilising the RANS and the *k* – ϵ model. A pressure-based solver, the SIMPLE algorithm, was used to solve the problem consecutively. The simulation was accomplished after 300 iterations.

Regarding the post-simulation processes, the solution output and data were extracted and transferred into a graphical form for observation and validation of the results. To extract the data, the line/rake setting in the ANSYS solver was utilised to produce four slices at the chosen positions across the domain. In this study, the slices were set up at 5D, 7D, 9D, and 25D downstream positions, following an earlier study conducted by Bakri [21] and Hoe [19] for validation purposes.

However, because the positions of the formed line depend on the model's axes and origin, we cannot directly specify any of the chosen values in the panel. This is because the origin of the model in this study is placed at the turbine in the third row as illustrated in Figure 5. Because the positioning of 5D to 25D must be subtracted from the first-row position (42.7 m). The final values of the 5D–25D line/rake to be created are listed in Table 4.

In addition, owing to the axes orientation, the direction of the endpoints (x, y, z) must be considered. This was influenced by the domain dimensions. Considering this context, the x-, y-, and z-axis endpoints are along the domain length, depth, and width, respectively. The x-, y-, and z-endpoint values may differ based on the model geometry and dimensions.

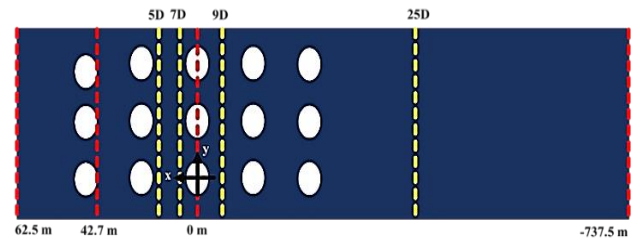


Figure 5 Schematic diagram for the model axis, origin, and extraction point (line/rake) used in this study

Table 4 Final value of 5D to 25D slices position

Position	Original Position (m)	Extraction Position (m)
5D	25	17.5
7D	35	7.5
9D	45	-2.5
25D	125	-82.5

3.0 RESULTS AND DISCUSSION

In this section, the wake behaviour in two different array configurations is discussed based on the velocity contour generated from the post-simulation task. Further analysis was performed on the velocity deficit based on the normalised velocity plotting.

3.1 15 Turbines Setup Using Set 1 Parameter (1.5D X 3.5D)

The results of the fluid flow interaction for both the HATT and VATT in the staggered and squared setups are shown in Figure 6. Both configurations have a greater velocity (yellow-green contour) in front of the device and a lower velocity (blue contour) after the fluid passes through the turbine. The low-velocity area behind the device was caused by energy loss when the flow interacted with the surface of the device. To sustain the volume flow rate continuity, the outer wake velocity of the closed channel must be greater than the free stream velocity, which is why the mean wake

velocity is slower. Furthermore, the flow surrounding the turbine is accelerated because of the blockage effect [6].

The results also demonstrate that despite their parallel behaviour, devices in the subsequent rows (i.e. row number two and beyond) of the squared-layout had substantially lower velocities than the staggered configuration turbines for both geometrical setups. This is due to two reasons. First, the wake from the first turbine's row of the squared setup is still recovering when the flow reaches the subsequent row. Second, the squared array does not exhibit flow acceleration phenomena owing to the blockage effect experienced by the staggered arrangement.

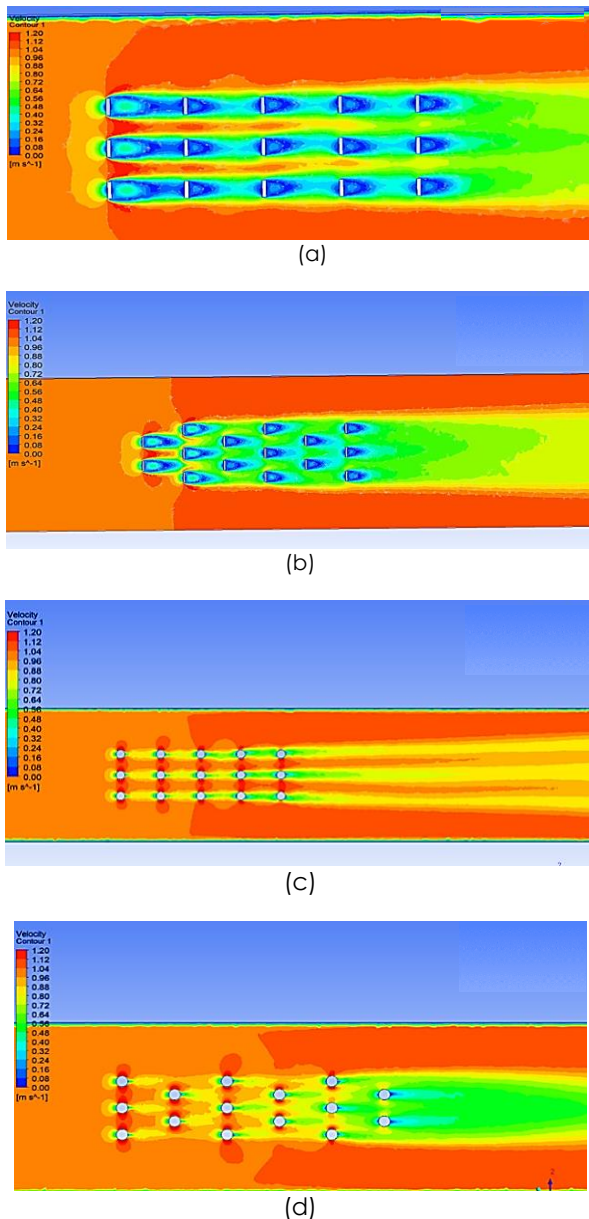
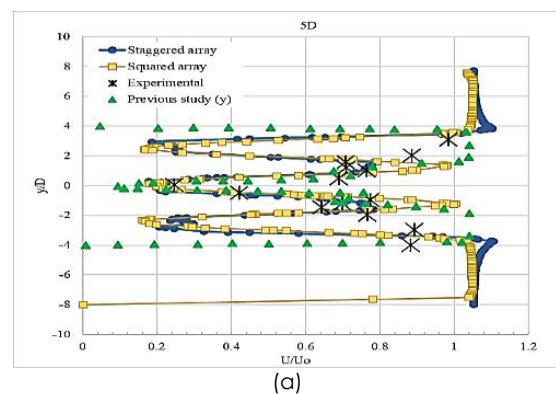


Figure 6 Velocity contour results for HATT and VATT model arranged in the staggered and squared array: (a) HATT model in squared array, (b) HATT model in staggered array, (c) VATT model in the squared array, (d) VATT model in a staggered array

To authenticate these findings, graphical plots, such as those in Figure 7 and Figure 8 are established to further explain the behaviour of the flow inside the domain. The plots present the normalised velocity of the HATT and VATT models in staggered and squared arrangements. Previous experimental and numerical research data by Harrison *et al.* [20] (i.e., experimental data denoted by black (x) marker in the plot legend), Hoe [19] (i.e., previous numerical study (y)), and Bakri [21] (i.e., previous numerical study (x)) were used for the validation purposes. In general, the figures demonstrate that the staggered and squared array normalised velocity at the centrelines follow the trend of the experimental data at each downstream position.

Considering Figure 7, the HATT model in both configurations has approximately the same normalised velocity at the centreline of the 5D downstream. In addition, the normalised velocity line for the HATT model lies within the left-hand side of the graph. It is also similar to the experimental results of previous studies. The percentage difference between the present study and the experimental data was quite small, at 27.26% and 28.23% for the staggered and squared arrays, respectively. Such a percentage deviation is observed owing to the inaccuracy of the RANS model. This does not consider the swirls generated from the blades, and the default material setting used for the device in the simulation may not be comparable to the real experimental conditions.

Subsequently, the normalised velocity at the centreline of the experimental and previous numerical research increased from 5D to 25D. However, there is no consistent normalised velocity trend near the centreline in the present study. Considering the staggered array, from 5D to 7D downstream, the velocity increases from 0.2 m/s to 0.4 m/s. However, at 9D downstream, the flow slows down and accelerates until 25D downstream. Regarding the squared array, the trend is a slower velocity at 7D downstream and a rising velocity from 9D to 25D downstream.



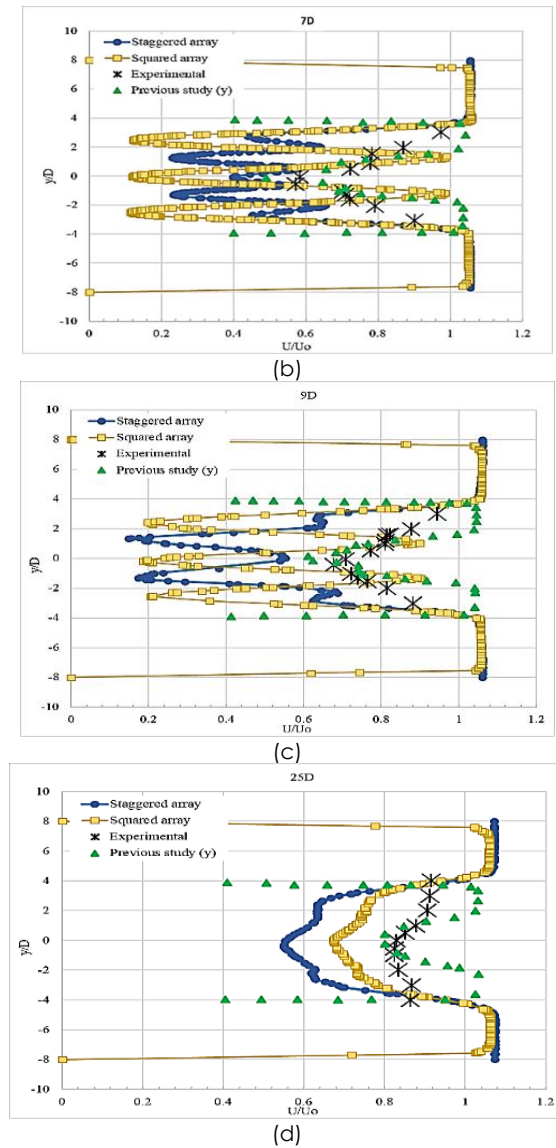


Figure 7 Comparison of the normalised velocity of the staggered and squared arrays for HATT model: (a) 5D downstream, (b) 7D downstream, (c) 9D downstream, (d) 25D downstream

Table 5 Percentage deviation comparison between the current study (HATT) and the experimental and previous numerical studies

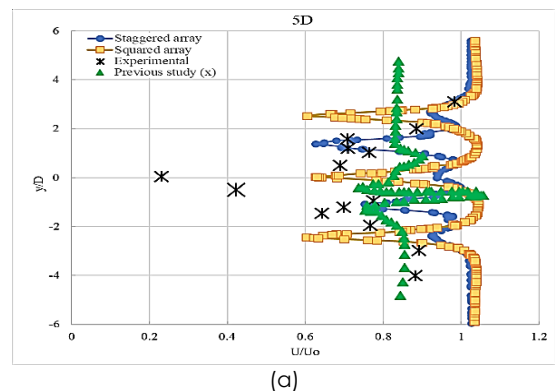
HATT : Percentage deviation (%) at downstream of turbine					
	Layouts	5D	7D	9D	25D
Current study vs experimental study	Squared	27.26	78.88	73.89	18.12
	Staggered	28.35	31.15	79.09	32.70
Current study vs previous study (y)	Squared	47.21	74.81	69.74	15.70
	Staggered	45.72	17.85	75.76	30.71

The percentage deviation between the experimental and previous numerical (HATT) studies, based on the extracted data from the midpoint position located behind the device at specific

intervals, is highlighted in Table 5. At both 9D and 25D downstream, the percentage deviation of the squared array was lower than the percentage deviation of the staggered array. A similar trend was observed when the current study was compared to a previous numerical study. Notably, the differences between the results of the current study and the experimental and previous numerical studies are significant, especially considering the percentage deviations.

These distinct trends in the normalised velocity of the data presented in Figure 7 and Table 5 are due to the different number of turbines used in the experimental and previous numerical studies. Studies by Hoe [19] and Harrison *et al.* [20] were conducted in a staggered configuration with three turbines which were different from those employed in the current study. The positions of 7D to 25D in the domain for the experimental and previous numerical studies also fall within the area where the flow is recovering and has fully recovered. Therefore, an increasing trend is observed. Considering the present study on a squared array, the decreased velocity at 7D downstream is due to its location in front of the turbine in the 3rd row of the domain. Considering Figure 6 (a), owing to the slower recovery of the second-row devices, wake merging occurs, resulting in less energy being collected by the downstream turbine. The lower velocity at the 9D downstream in the staggered array is due to greater turbulence intensity, and it occupies more space than the squared array.

Figure 8 compares the normalised velocity of the staggered and squared arrays for the VATT model. Regarding the plots presented, approximately all downstream flows in the current study possess a faster velocity. This is because most of the lines fall within the right-hand side of the graph. Considering Figure 8 (a) and (b), regarding both arrangements, it is observed that there is acceleration in the velocity from 5D to 7D downstream. After reaching the 9D downstream, the velocity starts to decrease. As the flow reached the 25D downstream position, the normalised velocity for the model in the squared arrangement increased. However, the velocity for the model in the staggered array was observed to further decelerate.



(a)

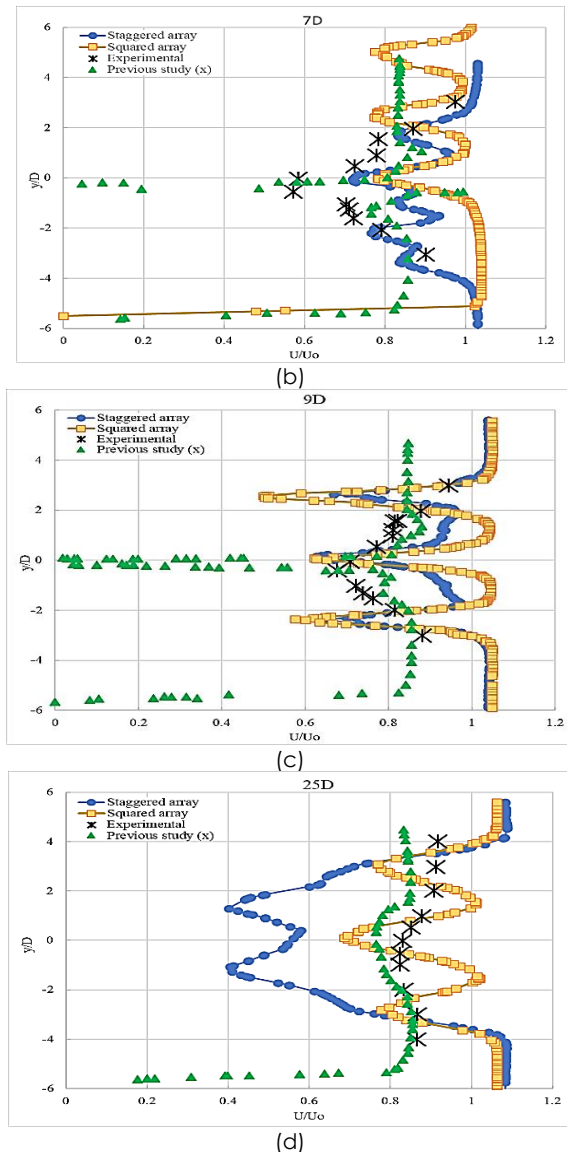


Figure 8 Comparison of the normalised velocity of staggered and squared array for VATT model: (a) 5D downstream, (b) 7D downstream, (c) 9D downstream, (d) 25D downstream

This can be explained by referring to the velocity contour results presented in Figure 6 (c) and Figure 6 (d). Considering the contour plot, the green contour behind the turbine is substantially shorter at 5D–7D downstream than at the 9D downstream. The extension of the length of the green contour further downstream is due to the slower velocity that the row receives from the upper row turbine. Consequently, the flow merges and recovers more slowly downstream.

Further analysis can be conducted by considering the percentage deviation (VATT study) which is tabulated in Table 6. The table reveals that the percentage deviations for both the staggered and squared arrays are higher when compared to the experimental data, and they are lower when compared to previous numerical studies. Subsequently, from 7D to 9D downstream, the gap between the normalised velocity of the current study

and that of the experimental study decreases. Hence, the percentage deviation between the two studies also decreases. This indicates that up to 9D downstream, the velocity starts to decrease gradually along with the downstream.

The differences between the results of the current study and the experimental and previous numerical studies are quite significant, especially considering the percentage deviations due to some changes in the layout parameters. Although both arrays contain the same number of devices in the domain, the staggered array includes six rows of turbines owing to its configuration of 3-2-3-2-3-2, with a total of 15 devices. However, the squared array includes only five rows of three turbines each. The 25D downstream is positioned after the last row of turbines in both the square and staggered arrays. Because the staggered array contains an additional row owing to its configuration, it has a smaller gap between the last row and 25D downstream than the squared array. Therefore, at the 25D downstream, the model in the staggered array experienced a slower velocity recovery owing to the presence of an additional row in the setup.

Table 6 Percentage deviation comparison between the current study (VATT) and the experimental and previous numerical studies

VATT : Percentage deviation (%) at downstream of turbine					
	Layouts	5D	7D	9D	25D
Current study vs experimental study	Squared	63.45	33.46	7.41	15.49
	Staggered	62.95	24.38	6.50	51.29
Current study vs previous study (y)	Squared	47.21	74.81	69.74	15.70
	Staggered	45.72	17.85	75.76	30.71

3.2 15 Turbines Setup Using Set 2 Parameter (3.0D X 7.0D)

Figure 9 illustrates the velocity contour findings for the HATT and VATT models using the staggered and squared setup for 3.0D X 7.0D spacing which is doubled from the previous setup. In general, the velocity contour shows that both configurations effectively follow the flow profile characteristics based on the conservation of momentum principle. The contour plots show that both models demonstrate a similar fluid flow pattern, where the velocity accelerates when encountering the turbine surface. When the incoming flow passes through the surfaces of the devices, energy is lost, causing a slow flow zone to form behind the turbines.

Both array setups exhibit distinct wake characteristics from each turbine, with no inter-row wake merging at the upper stream. This excludes the squared arrangement of the HATT model shown in Figure 9 (a), where inter-row wake merging occurs immediately after the first row. Moreover, after the fourth row, the flow in the downstream turbine starts to converge in the squared arrangement of the VATT

model as displayed in Figure 9 (c). This occurs because of turbulent mixing when the flow experiences a reduction in velocity after passing through the turbine as demonstrated by the green zone on the contour.

This is because of the device arrangement, where the downstream device of the squared array is aligned with the upstream devices. Increasing the gap between the rows may assist in preventing merging. There is no wake interference from the upstream turbine owing to the larger longitudinal separation. Although the spacing between the turbines is proportional to the width and length of the domain, the separation should not be simply expanded because the simulation time may be longer in a complex domain.

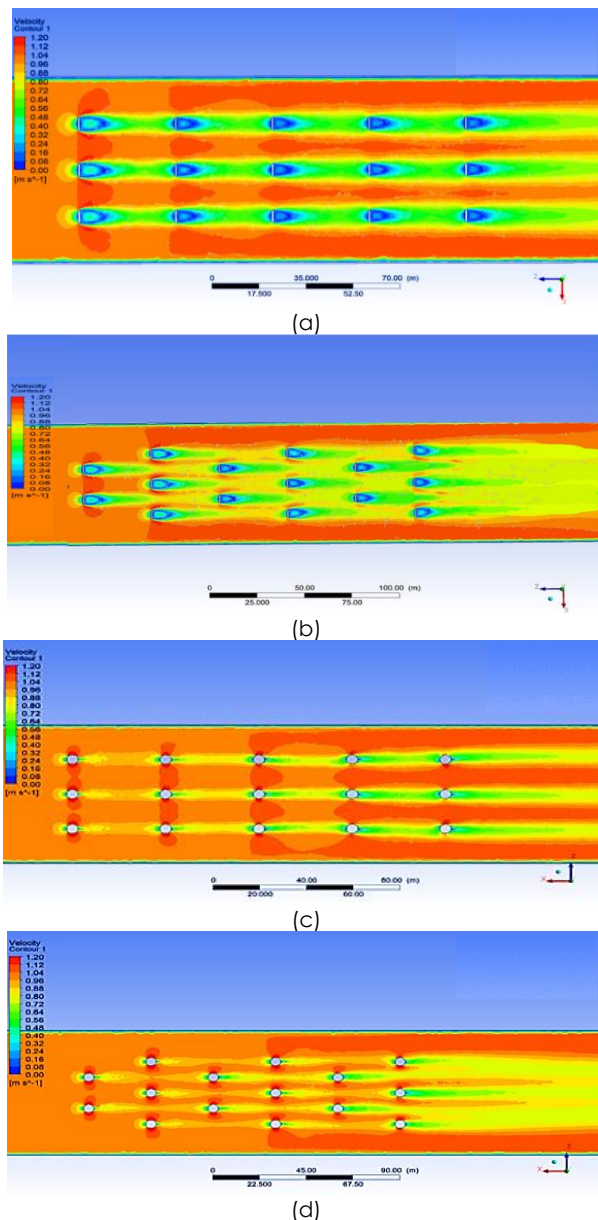
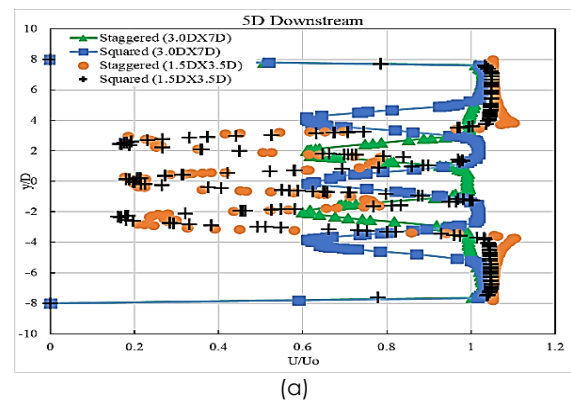


Figure 9 Velocity contour results for HATT and VATT model arranged in the staggered and squared array: (a) HATT model in the squared array, (b) HATT model in the staggered array, (c) VATT model in the squared array, (d) VATT model in a staggered array

Another notable observation from the figure is the flow dispersion area on the side of the turbine model. Considering Figure 9 (a) and (c), the models in the squared configuration have a larger dispersion area on the side of the cylinders. The shape of the cylinder allows the fluid to circulate around the curved area of the cylindrical turbines. This decreases the fluid velocity. The fluid velocity and pressure diminish down the cylinder side, influencing the near-wake zone downstream. However, the surface of the cylinder geometry allows the fluid velocity to spread aggressively throughout the side of the cylinder in the squared array. Consequently, the fluid has more turbulent kinetic energy, while passing through the turbine. A higher turbulence kinetic energy and pressure will influence the wake recovery, affecting how quickly the domain recovers.

On the contrary, another analysis via graph plotting is established to further discuss the flow behaviour in the domain for the HATT and VATT model as presented in Figure 10 and Figure 11, respectively. These figures compare the normalised velocity of the models in staggered and squared arrays with spacing of Set 1 and 2. Considering the plots, the flow in the HATT model with a larger spacing experiences a velocity reduction from 5D to 9D downstream positions as demonstrated in Figure 10 (a), (b), and (c).

Despite the depletion of velocity, the flow still manages to reach equilibrium faster than the flow in the model with a smaller spacing. This is because the normalised velocity of the model in a larger separation surpasses the normalised velocity of the model with a smaller separation. This may be caused by the existence of higher intensity turbulence behind the turbine in the model with a smaller separation as previously displayed in Figure 6 (a) and (b). At approximately 25D downstream, the velocity is increased because the wakes from the upstream and downstream devices progressively merge to form a single, larger, and longer wake. This increases the recovery distance before the flow finally recovers to reach the ambient velocity.



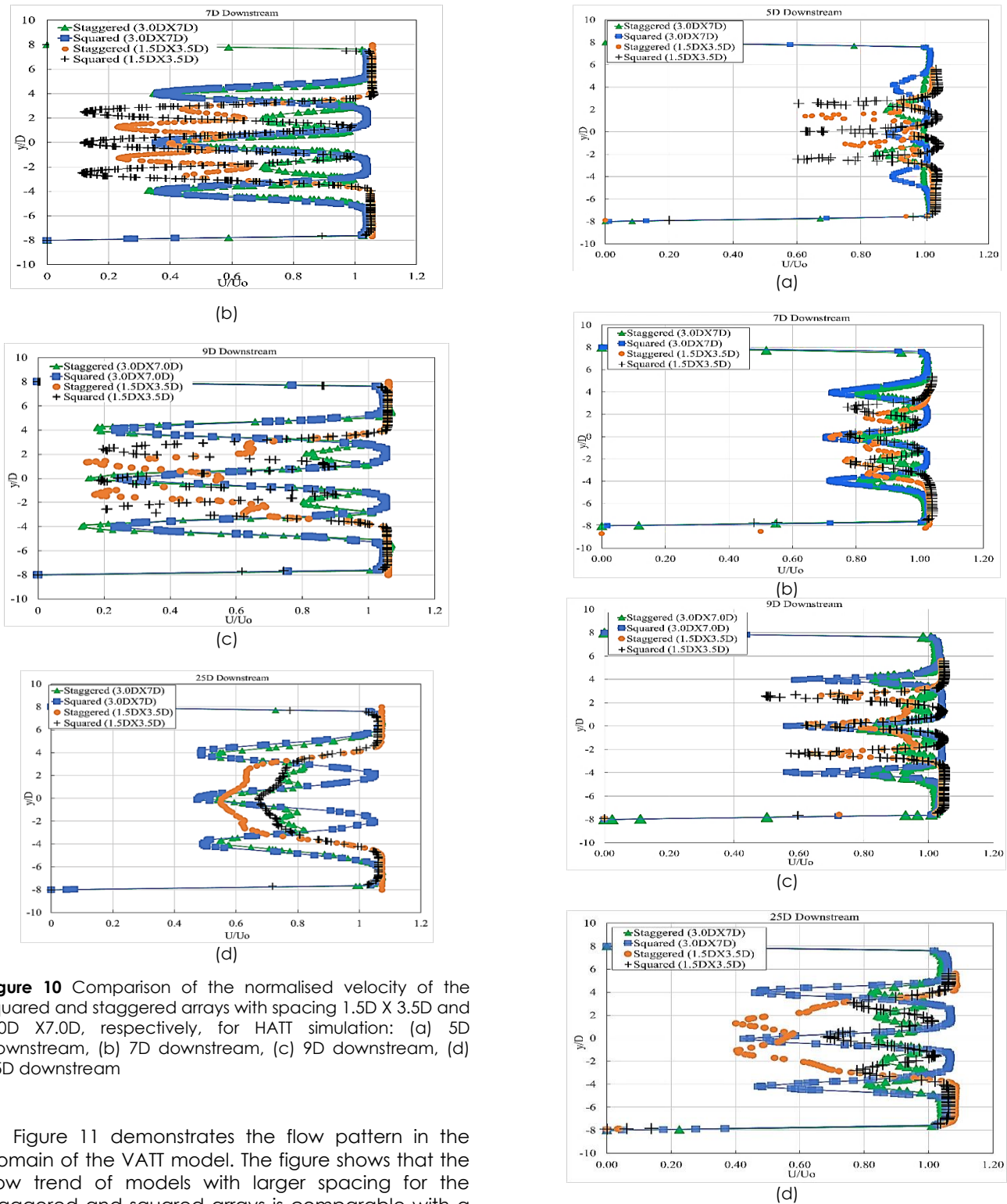


Figure 10 Comparison of the normalised velocity of the squared and staggered arrays with spacing 1.5D X 3.5D and 3.0D X 7.0D, respectively, for HATT simulation: (a) 5D downstream, (b) 7D downstream, (c) 9D downstream, (d) 25D downstream

Figure 11 demonstrates the flow pattern in the domain of the VATT model. The figure shows that the flow trend of models with larger spacing for the staggered and squared arrays is comparable with a reduction in velocity further downstream. The velocity contour in Figure 9 (c) and (d) demonstrates this behaviour. The green contour behind the turbine expands across the domain in both the staggered and squared layouts.

Figure 11 Comparison of the normalised velocity of the squared and staggered arrays with spacing 1.5D X 3.5D and 3.0D X 7.0D, respectively, for VATT simulation at: (a) 5D downstream, (b) 7D downstream, (c) 9D downstream, (d) 25D downstream

Turbulent mixing causes slower velocities, resulting in a slower downstream wake recovery. Excluding the 25D downstream, models with greater spacing showed higher normalised velocity toward the centreline. Upstream, the flow reaches equilibrium faster when a greater spacing (5D to 9D) is used. It is also clear from the 25D plot that the model with greater spacing takes a longer time to recover to its ambient velocity when compared to the smaller spacing arrangement.

Table 7 compares the percentage deviations for the two spacing setups in the VATT model. The percentage deviations for both models share the same pattern. The percentage deviation was high at 5D downstream, and it decreased at 7D downstream. Regarding the squared array, the percentage deviation continued to decrease at 9D downstream and started to increase at 25D downstream. In contrast, considering the staggered arrays, the percentage deviation started to increase at 9D downstream and continued to increase at 25D downstream. This can be attributed to the higher turbulence intensity in the downstream region as discussed previously. The table shows that spacing plays an important role in tidal turbine performance, where the model with larger spacing presents better results and is more likely to be implemented in shallow-water conditions.

Table 7 Percentage velocity deviation comparison between VATT model with small spacing (1.5D X 3.5D) and VATT model with bigger spacing (3.0D X 7.0D)

Layouts	Downstream			
	5D	7D	9D	25D
Squared	29.54	9.74	9.60	38.83
Staggered	26.43	9.72	20.47	52.52

4.0 CONCLUSION

An array of tidal devices for shallow-water applications is theoretically modelled and evaluated. Between the HATT and VATT simulations, the VATT results indicate an outstanding output because they can outperform the HATT turbines under certain conditions. The VATT has a quicker wake recovery, which is preferred in shallow-water applications. Comparing the staggered and squared arrays, the staggering array performs better in both the VATT and HATT simulations. In addition, a greater spacing setup appears to be a better choice because it reduces the magnitude of turbulent mixing with devices in subsequent rows.

Overall, a VATT turbine array with greater spacing is the best option for use in open water in Malaysia. However, in real applications, the spacing is most likely to be influenced by a combination of factors, such as the deployment area, turbine size, and current velocity of the chosen region. In summary, this study achieves the set objectives, which are to investigate

the influence of tidal turbine array configuration on shallow water conditions and to propose the optimal array configuration for shallow water applications.

In the future, the cylinder and disc objects used in this study may be replaced with a full-scale blade design. This study may involve static and dynamic blades to assess the flow characteristics and device performance. Changes in the rotation of the turbines in the rows may also be investigated to determine the actual flow dynamics between the rows of the devices. Additionally, various turbulence model approaches can be explored to determine their influence on the wakes generated and the interactions between the rows of devices.

Acknowledgment

The authors gratefully acknowledge the financial support received from the Ministry of Higher Education, Malaysia, through the Fundamental Research Grant Scheme for Research Acculturation of Early Career Researchers (FRGS-RACER)–RACER/1/2019/TK07/UNIMAP/1.

References

- [1] D. Satrio, I. K. A. P. Utama, and Mukhtasor. 2016. Vertical Axis Tidal Current Turbine: Advantages and Challenges Review. *Proceeding Ocean. Mech. Aerosp. -Science Eng.* 3(July): 64-71. [Online]. Available: <http://isomase.org/OMase/Vol.3-2016/Section-1/3-7.pdf>.
- [2] F. Mushtaq, W. Maqbool, R. Mat, and F. N. Ani. 2013. Fossil Fuel Energy Scenario in Malaysia-prospect of Indigenous Renewable Biomass and Coal Resources. Doi: 10.1109/CEAT.2013.6775632.
- [3] N. Gomesh, I. Daut, M. Irwanto, Y. M. Irwan, and M. Fitra. 2013. Study on Malaysian's Perspective Towards Renewable Energy Mainly on Solar Energy. *Energy Procedia*. 36: 303-312.
- [4] K. S. Lee and L. Y. Seng. 2009. Simulation Studies on the Electrical Power Potential Harvested by Tidal Current Turbines. *J. Energy Environ.* 1: 18-23.
- [5] I. K. A. P. U. E. Septyaningrum, R. Hantoro and N. A. S. J. Prananda, G. Nugroho, A. W. Mahmashani. 2017. Performance Analysis of Multi-row Vertical Axis Hydrokinetic Turbine-straight Blade Cascaded (VAHT-SBC) Turbines Array. *J. Chem. Inf. Model.* 110(9): 1689-1699. Doi: <https://doi.org/10.15282/jmes.13.3.2019.28.0454>.
- [6] H. Y. Chong and W. H. Lam. 2013. Ocean Renewable Energy in Malaysia: The Potential of the Straits of Malacca. *Renewable and Sustainable Energy Reviews*. 23: 169-178. Doi: 10.1016/j.rser.2013.02.021.
- [7] F. Behrouzi, M. Nakisa, A. Maimun, and Y. M. Ahmed. 2016. Renewable Energy Potential in Malaysia: Hydrokinetic River/Marine Technology. *Renewable and Sustainable Energy Reviews*. 62: 1270-1281. Doi:10.1016/j.rser.2016.05.020
- [8] A. Roberts, B. Thomas, P. Sewell, Z. Khan, S. Balmain, and J. Gillman. 2016. Current Tidal Power Technologies and Their Suitability for Applications in Coastal and Marine Areas. *J. Ocean Eng. Mar. Energy*. 2198-6452. Doi: 10.1007/s40722-016-0044-8.
- [9] M. De Dominicis, R. O'Hara Murray, and J. Wolf. 2017. Multi-scale Ocean Response to a Large Tidal Stream Turbine Array. *Renewable Energy*. 114(Part B): 1160-1179.
- [10] P. Ouro, L. Ramírez, and M. Harrold. 2019. Analysis of Array

- Spacing on Tidal Stream Turbine Farm Performance using Large-Eddy Simulation. *Journal of Fluids and Structures*. 91: 102732.
- [11] D. Mehta, A. H. van Zuijlen, B. Koren, J. G. Holierhoek, and H. Bijl. 2014. Large Eddy Simulation of Wind Farm Aerodynamics: A Review. *Journal of Wind Engineering and Industrial Aerodynamics*. 133: 1-17.
- [12] F. Attene, F. Balduzzi, A. Bianchini, and M. Sergio Campobasso. 2020. Using Experimentally Validated Navier-stokes CFD to Minimize Tidal Stream Turbine Power Losses Due to Wake/Turbine Interactions, *Sustain*. 12(21): 2-26. Doi: 10.3390/su12218768.
- [13] E. W. Purnomo and D. P. Ghosh. 2018. Identifying Shallow Water Flow in Offshore Malaysia using Multicomponent Data and FWI Approach. Paper presented at the Offshore Technology Conference Asia, Kuala Lumpur, Malaysia, March 2018. Doi: <https://doi.org/10.4043/28276-MS>
- [14] P. Ouro, M. Harold, T. Stoesser, and P. Bromley. 2017. Hydrodynamic Loadings on a Horizontal Axis Tidal Turbine Prototype. *Journal of Fluids and Structures*. 71: 78-95.
- [15] D. Fallon, M. Hartnett, A. Olbert, and S. Nash. 2014. The Effects of Array Configuration on the Hydro-environmental Impacts of Tidal Turbines. *Renew. Energy*. 64: 10-25. Doi: 10.1016/j.renene.2013.10.035.
- [16] C. D. Scott-Pomerantz. 2004. The K-Epsilon Model in Theory of Turbulence. University of Pittsburgh, Pittsburgh.
- [17] D. Kuzmin, O. Mierka, and S. Turek. 2007. On the Implementation of the k - ϵ Turbulence Model in Incompressible Flow Solvers based on a Finite Element Discretisation. *Int. J. Comput. Sci. Math.* 1(2-4): 193-206. Doi: 10.1504/ijcsm.2007.016531.
- [18] B. Johnson, J. Francis, J. Howe, and J. Whitty. 2014. Computational Actuator Disc Models for Wind and Tidal Applications. *Journal of Renewable Energy*. Doi: 10.1155/2014/172461.
- [19] B. C. Hoe. 2019. The Influence of Tidal Turbine In Array Configuration on the Wake Formation For Shallow Water. Universiti Malaysia Perlis.
- [20] M. E. Harrison, W. M. J. Batten, L. E. Myers, and A. S. Bahaj. 2010. Comparison between CFD Simulations and Experiments for Predicting the Far Wake of Horizontal Axis Tidal Turbines. *IET Renew. Power Gener.* 4(6): 613-627. Doi: 10.1049/iet-rpg.2009.0193.
- [21] A. Bakri. 2020. Numerical Assessment of Vertical Axis Marine Current Turbines Performances in Shallow Water: A Case Study for Malaysia. Universiti Malaysia Perlis (UniMAP).